4D printing of continuous flax-fibre based shape-changing hygromorph biocomposites: Towards sustainable metamaterials

A Le Duigou, T Fruleux, R Matsuzaki, G Chabaud, M Ueda, M Castro

Materials & Design 211 (2021) 110158

Contents lists available at ScienceDirect

Materials & Design

journal homepage: www.elsevier.com/locate/matdes

4D printing of continuous flax-fibre based shape-changing hygromorph biocomposites: Towards sustainable metamaterials

A. Le Duigou [a,*], T Fruleux [a], R. Matsuzaki [b], G. Chabaud [a], M. Ueda [c], M. Castro [a]

[a] Univ. Bretagne Sud, UMR CNRS 6027, IRDL, F-56100 Lorient, France
[b] Tokyo University of Science, 2641 Yamazaki, Noda 278-8510, Chiba, Japan
[c] Nihon University, 1-8-14 Kanda-surugadai, Chiyoda 101-8308, Tokyo, Japan

HIGHLIGHTS

- 4D printing of Hygromorph BioComposites was performed.
- Soft matrix enhance actuation of Hygromorph biocomposite.
- Layer Height (LH) allows for local control of thickness and stiffness ratio.
- Interfilament Distance (IDp) allows for variable composite stiffness.
- Simple compliant mechanism via localized microstructure change are proposed.

GRAPHICAL ABSTRACT

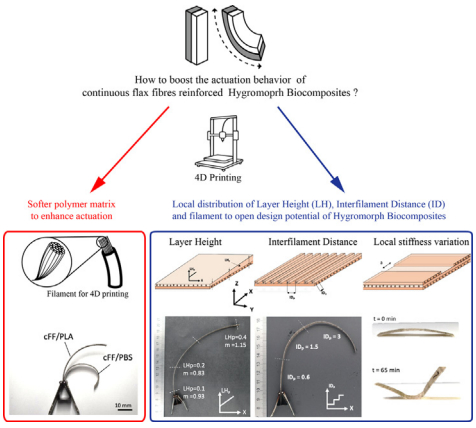

ARTICLE INFO

Article history:
Received 14 May 2021
Revised 30 August 2021
Accepted 9 October 2021
Available online 11 October 2021

Keywords:
4D printing
Biocomposites
Natural fibres
Morphing
Moisture

ABSTRACT

4D printing focus on the integration of a targeted morphing function by controlling the properties and the architecture of the materials.

The present work evaluates the potential of tailoring 4D printing to Hygromorph BioComposite (HBC), which paves the way for the construction of a new generation of sustainable shape-changing metamaterials with a sequential response. HBCs are made of continuous flax fibres that have been proven to be relevant for actuation and thus 4D printing due to their hygromorphism function.

The morphing performance of HBCs can be boosted by selecting an appropriate matrix. The soft Poly Buthylene Succinate (PBS) matrix showed a 92% increase in responsiveness and 500% increase in reactivity compared to the Poly Lactic Acid (PLA)/Flax HBC.

4D printing with Layer Height (LH) control within layers allows for complex actuation potential with a local control of the thickness and stiffness ratio. The Interfilament Distance of the 0° oriented passive layer (IDp) offers the opportunity to achieve non-uniform reactivity and responsiveness for autonomous smart surfaces.

Finally, the programming of the spatial distribution of the flax yarn can be combined with heterogeneities. As an illustration, simple compliant mechanism via localized microstructure changes is proposed.

* Corresponding author.
E-mail address: antoine.le-duigou@univ-ubs.fr (A. Le Duigou).

https://doi.org/10.1016/j.matdes.2021.110158
0264-1275/

1. Introduction

4D printing is a recent trend (since 2013) that aims to develop 3D-printed architected materials or metamaterials that can change their shape or properties according to external stimuli (temperature, ultra-violet light, humidity, electric and magnetic field) [1,2,3] based on a predetermined morphological transformation. To control this functionality, specific functional materials are embedded at the desired locations [4]. Currently, research on 4D printing focuses mainly on the development of metamaterials that change from 2D to 3D [5,6,7]. The transition from 2D to 3D shape allows flat constructions to fold into geometrically complex 3D objects [8,9]. A wide range of materials is currently used for this purpose, such as Shape Memory Polymer (SMP) [10,11,12,13], Electro-Active Polymer (EAP) [14], hydrogel [15] and recently Hygromorph BioComposites (HBC) [16,17,18].

Hygromorph BioComposites (HBC) are among the few sustainable smart materials based on local renewable resources with a low environmental burden [19]. They are both autonomous sensors and actuators that require no additional energy for mechanical or electronic control. In this sense, they follow the paradigm of closed-loop 4D-printed structures that integrate 3D-printed sensors, 3D-printed actuators, and feedback information to achieve the functional target in time while interacting with uncertain environments in real-time [4].

Indeed, they work due to the hygroscopic anisotropic properties (moisture-induced reduction and expansion of stiffness) of natural fibres ultrastructure and composition [20] and an asymmetrical architecture biologically inspired by the scales of the pine cone [16,20]. Their application can be envisaged in reconfigurable medical devices [21], sensors and actuators [22], soft robotics [23] and self-deployable structures, e.g., in architecture and building construction with environmentally-responsive zero-energy façade systems [24]. Compared to shape-changing metamaterials made with pure matrix, HBC with continuous natural fibres delivers significantly higher actuation authority due to their higher stiffness and strength [20,25]. In addition, the use of continuous fibres allows for better control of the anisotropic property and thus the actuation direction [26].

Current 4D printed HBC are mainly based on off–the-shelf short natural fibre composites [27,28]. To enlarge actuation potential, customized material formulation and continuous fibres should be preferred over discontinuous fibers, as it is difficult to properly align short fibres [29]. Very few works are available on 4D printed shape-changing metamaterials based on continuous fibre composites. As far as we know, the only works are from le Duigou et al [30] and Wang et al. [26]. The latter have evidenced that complex, thermally-induced shape change could be created by controlling the deposition of continuous carbon fibres in a PolyAmide-6 (PA6) matrix while allowing encouraging mechanical properties given by carbon fibre stiffness. Le Duigou et al [30] have shown that multiple stimuli-responsive continuous carbon fibre/PA composite materials can be proposed (electro-thermo-hygro responsive). Currently, a biobased and sustainable alternative is still lacking despite the global environmental context. In addition, no work has been done yet on 4D printing of moisture-induced actuators with continuous fibre-reinforced composites, and even less with natural fibres. Continuous flax fibre biocomposites have been successfully 3D printed for semi-structural applications and have evidenced drastically better mechanical performances than short fibre biocomposites [31]. These properties can be tailored by selecting slicing parameters during the design stage to achieve a targeted architecture [32].

Thus, deeper insights into the relationship between bio-inspired meso-structures and sequential spatio-temporal morphing of continuous flax HBC should be proposed.

For example; hygromorphic biological actuators such as the pine cone [13,32] present local thickness variations that alter their local bending stiffness, while hierarchically porous cell-wall structures enhance water diffusion by capillarity [33]. In these structures, the porosity network acts as a moisture diffusion pathway rather than a mechanical defect [20]. The porosity network and channel formation are influenced by the interfilament distance. For example, Gladman et al. [15], on polyacrylamide hydrogel / short cellulose fibre composites, showed that water diffusion is promoted by increasing filament spacing due to an increased surface-to-volume ratio and porosity.

During 4D printing, the local variation in the thickness of the printed sample is mainly adjusted by the number of printed filaments [7], but rarely discussed in terms of variation of Layer Height (programmed distance between the nozzle and the print bed). This point deserves investigation as it opens the design space of the related shape-changing materials.

In addition, localized heterogeneities in the spatial distribution of materials can give rise to a transition from structural bending to folding. Better control of the final shape of morphing structures can be achieved [34,35]. For example, Mao et al. [36] designed folding structures using a multi-material 3D printer where each hinge is specifically designed with polymers whose behaviour is time and temperature dependent (glass transition temperature). Zolfagharian et al. [37] evidenced that the spatio-temporal response of a 4D printed self-folding PS/Chitosan hydrogel ink actuator can be controlled by the hinge pattern. Again, the available research on understanding the relationship between the mesostructure induced by the printing parameters and the opportunity to complexify the local response is rarely applied to moisture-induced actuation with continuous fibres composites, and even less with natural fibres.

The purpose of the present article is, for the first time, to combine the potential 4D printing for 2D to 3D transformation with the use of a high performance and sustainable HBC made from continuous flax fibres. First, the material selection is discussed in terms of matrix stiffness with characterization of the hygro-elastic and actuation properties of biocomposites having a “stiff” Poly Lactic Acid (PLA) and a “soft” Poly Buthylene Succinate (PBS) matrix.

Then, the mesostructured control (ply scale) given by the 4D printing parameters (Layer Height LH and Interfilament Distance ID) and its potential to tune HBC actuation will be investigated within the framework of Timoschenko’s equations and their parameters (n, m and $\beta.\Delta Mt$).

Finally, stiffness control using a gradual and local architecture will be presented on a printed specimen to illustrate the mesostructural effects on the range of HBC spatio-temporal responses.

2. Materials and methods

2.1. Materials

Continuous flax fibres (cFF) organized in yarns were provided by SAFILIN (France). They possess a low twist (320 Turn/meter) and a low linear density of 68 Tex. These two factors ensure favorable mechanical properties [38]. PolyLactic Acid Ingeo™ 3260HP (PLA) was supplied by NatureWorks® (USA). Polybutylene Succinate (PBS) Bionolle 1020 MD was supplied by Showa Denko (Tokyo, Japan).

2.2. Filaments production

The filaments were produced by a co-extrusion process combining polymer coating of the flax yarn and impregnation. Photographs and more information can be found in our previous articles discussing cFF/PLA Biocomposites for 3D printing [39,32]. The filament diameter was approximately 500 μm, in a range similar to that used in studies of continuous synthetic fibre reinforced composites. Table 1 reports the extrusion parameters that were used for PLA and PBS-coated continuous flax fibres filaments. Determined by image analysis (5 replicates), the fibre volume content was 25.9 ± 1.1 %.

2.3. Production of composites by fused filament fabrication (FFF)

A Prusa MK3s printer was customized. To feed the nozzle with continuous filament, an extrusion motor has been installed to control the amount of filament printed. Then, a flat head nozzle was used to compress the filament and drive it during printing. The temperature of the nozzle and heating plate were set at 195 °C and 60 °C for PLA/cFF and 135 °C and 20 °C for PBS/cFF, respectively. The printing speed was set at an optimized speed of 6 mm/s which was based on preliminary tests.

All samples were printed with a rectilinear filling pattern. The print trajectory is controlled by a manually written G-code, then transferred to Repetier Host to control the printer.

2.4. Characterization of the mechanical properties

Tensile samples geometry is settled at Length (L): 125 mm; Width (W): 10 mm and thickness (t): 1 mm. Tensile tests were performed on longitudinally (0°) and transversely (90°) printed samples following ISO 527-4 standards. The Layer Heights applied to the tensile test specimens (0 or 90°) are the same as those used for the bilayer (*i.e.* 0.2 mm). The Interfilament distance (ID) is kept at 0.6 mm, the Layer number (LN) is equal to 5, and the number of turns is 18 for the longitudinal samples (0°) and 75 for the transverse samples, similarly to [32]. For the transverse samples, the edges have been machine-milled. The tensile modulus E_1 was determined over a range of strains between 0.05 % and 0.1 % according to the procedure suggested by Shah et al. [40]. The tensile displacement rate was set at 1 mm/min, and five specimens were systematically tested for each characterization.

2.5. Microstructure observations

The microstructures of the printed parts were observed by optical microscopy (Olympus BX51) at different magnifications (x5, x10, x20). The samples were cut, coated with epoxy resin and finally polished with abrasive paper and diamond paste to obtain a clean and flat observation surface. For larger parts, a binocular microscope was used (Leica MZ16 binocular with 16:1 magnification and 840 LP mm − 1 resolution).

Table 1
Extrusion parameters to produce PLA coated continuous flax filaments.

	Flax/PLA yarn filament	Flax/PBS yarn filament
Die size (mm)	0.6 (diameter) × 20 (length)	0.6 × 20
Extruder temperature (°C)	180	160
Die temperature (°C)	190	170
Oven temperature (°C)	120	Room temperature
Consolidating system (mm)	40 × 7	40 × 7
Puller speed (m/min)	1	1
Extrusion speed (rpm)	5	2

2.6. Moisture sorption and hygroscopic expansion

Three samples per batch (PLA/cFF and PBS/cFF) were immersed in deionized water until a constant weight was obtained. Their geometry was settled at L: 70 mm; W: 25 mm and t: 1 mm. The samples have been periodically removed and wiped of water for weighing and characterization. The percentage gain M_t at any time t has been calculated as follows:

$$M_t(\%) = \frac{W_t - W_0}{W_0} \times 100 \quad (1)$$

where W_t and W_0 are the weight of sample after water exposure and the weight of the dry material before immersion, respectively. The maximum moisture absorption M_∞ is calculated as the average value of five consecutive measurements. Desorption of saturated samples was measured under laboratory conditions (RH = 50% and T = 23 °C) by continuously recording changes using a weighing device with an accuracy of 10^{-4} g.

For hygroexpansion measurements, ten lines were drawn on the sample longitudinally and transversally to the fibre orientation to ensure that swelling measurements were always performed at the same location. Measurements were done with a digital optical microscope (Keyence VHX-100, VHX-900 lens: VH-Z20W, VH-Z450). The results were then arithmetically averaged.

2.7. Bending curvature analysis

The bending curvature of the HBC was evaluated during immersion by periodically taking pictures of one side of the clamped sample (HD Pro c920 Logitech®, 15 Megapixels).

Each sample is clamped with a binding clamp on a very small length of the sample to reduce stress concentration on the bilayer, and therefore leaving a free length of approximately 70 mm. Image analysis is performed using ImageJ® software (National Institute of Health, USA). The deformed shape is here assumed to be circular arc and the curvature is therefore measured by fitting the temporal evolution of the sample to a 'circle' function. The bending curvature (κ) is calculated according to the radius of the fitted circle.

3. Results and discussion

3.1. Influence of selected materials on the morphing of hygromorph BioComposites

Compared to wood-based hygromorph materials, hygromorph biocomposites result in a longer equalization time because they do not have the same vascular capacity as wood tissue. In addition, the thermoplastic polymer material limits the moisture absorption [27] while the selection of natural fibres based on their composition and architecture controls the actuation potential [20]. Therefore, the formulation of the materials is of great importance. This is one of the main advantages of hygromorph biocomposites compared to wood-based hygromorphs.

Thus, in addition to the cFF/PLA hygromorphs where the matrix is considered stiff, the cFF/PBS counterparts are evaluated as the tensile properties of the matrix are drastically different (E_{PLA} = 3.6 GPa ; ε_{PLA} = 3% [41] and E_{PBS} = 0.64 GPa ; ε_{PBS} = 264% [42]). The mechanical, hygroscopic and actuating properties of the hygromorphic biocomposites cFF/PLA and cFF/PBS are gathered in Table . Due to the continuous reinforcement combined with a low linear weight (68 Tex) and the selection of flax fibers, the longitudinal tensile properties of the biocomposites have evidenced high values

compared to the literature data on 3D-printed short fiber biocomposites [43]. They are in the same range as those observed for MAPP/Flax with a similar fiber fraction [25] but are obviously lower than those of MAPP/Flax biocomposites containing 60% by volume of fibers [44]. The production of filaments with continuous natural fibers is still in its early stages and several optimizations should be made as the volume fraction of the fiber is currently still somewhat limited.

Transverse moduli are low and mainly influenced by matrix moduli, fibre content, microstructure heterogeneities and printing induced defects. Substitution of PLA matrix with PBS reduces longitudinal and transverse stiffness by 30% and 75 %, respectively, due to the high contribution of the matrix (Table) in composites with a moderate fiber content.

Based on a PLA matrix, the anisotropic ratio is considerably higher than that of 3D-printed short-wood-fibers (V_f = 15% vol) reinforced PLA biocomposites (n = 1.5 [16]) but lower than that of continuous flax fiber (V_f = 60% vol) reinforced maleic-anhydride-grafted-polypropylene (MAPP/Flax) biocomposite (n = 17.3 [20]). CFF/PBS biocomposites show a higher anisotropic ratio, mainly due to a great reduction in transverse stiffness. Although increasing in the ratio *n* reduces the actuation potential (Figure. b), driving the anisotropic properties allows better control of the directionality of the shape change and improves the building potential of multi-curvature system, creating constraints for longitudinally oriented fibers and swelling for transverse fibers [27]. As evidenced by Wang et al. [26] on continuous carbon fibers/PA6, the final direction of curvature is the angular bisection line of the acute angle between the crossing fiber bundles.

Then, the hygroscopic strains that drive actuation are drastically improved (+250%) compared to cFF/PLA counterparts. Indeed, free flax fibers can exhibit a radial hygroscopic expansion of about 21 ± 3% [45], thus a low stiffness matrix such as PBS appears to reduce the constraining effect on the flax fibers during sorption, allowing for a greater hygroscopic expansion of the embedded fibers and thus of the composites.

Actuation measurements were carried out on cFF/PLA and cFF/PBS samples whose stacking sequence was set to a total number of two layers to minimize the bending stiffness (Table 2). Comparison of the theoretical curvature with that obtained experimentally confirms that the use of Timoschenko's equations to design hygromorph biocomposites with slender geometry is fairly reliable (error rates of 9% and 7% for cFF/PLA and cFF/PBS, respectively). Fig. 1.a, b, c and d show the cross-section and in-plane microstructure of cFF/PLA HBC after printing, cFF/PLA and cFF/PBS HBC before and after immersion in water, respectively.

Microscopic observations of the HBC microstructure highlight the control of the microstructure with some interlaminar and matrix porosities (Fig. 1.a), local misalignment of the yarn and local variations in the interfilament distance (Fig. 1.b). Overall, 4D-printing of hygromorph biocomposites with bilayer architecture and continuous flax fibers provides a much better actuation performance than that observed with HBC reinforced with short natural fibers. For example, short-wood-fibers/PLA-PHA (blend) hygromorph biocomposites have a maximal curvature of 0.012 ± 0.003 mm^{-1} [16]. This is mainly attributed to the higher fiber content, the different biochemistry and architecture of the fibers (lignin content and low MFA) and better control of the fiber orientation on the printed specimen.

The curvature analysis was performed by the difference between the initial curvature (RH = 50%) and the final curvature (immersion). Selection of the PBS matrix instead of PLA shows a 2-fold increase in responsiveness over the cFF/PLA that can be directly attributed to the higher transverse hygro-expansion of the cFF/PBS composite (Table 2).

To better understand the relationship between hygroexpansion, matrix stiffness and curvature actuation, the hygroscopic radial residual stresses generated within asymmetric laminates by moisture sorption are estimated using equation (2) [46]:

$$\sigma_{22} = \sigma_{radial} = \frac{E_{11}.E_{22}}{E_{11}+E_{22}} \frac{t}{\Delta\rho}\left(\frac{1}{2}+\frac{1}{24}(2+\frac{E_{11}}{G_{12}}+\frac{E_{22}}{G_{12}}\right) \quad (2)$$

With t the total thickness of the sample (t = 0.650 mm), $\Delta\rho$ the differential curvature radius ($\Delta\rho = \rho_{\text{after printing}} - \rho_{\text{after actuation}}$, E_{11} and E_{22} are the values of longitudinal and transverse modulus, G_{12} is the in-plane shear modulus of the laminate estimated by the rule of mixture using G_{flt} = 2500 MPa [47] and $G_m = \frac{Em}{2(1+\vartheta)}$. One obtained a radial compressive stress range of 31 and 17 MPa for cFF/PLA and cFF/PBS, respectively, confirming the lower constraining effect of PBS on the flax fibers. Although this may affect the load transfer between the fiber and the matrix as proposed elsewhere [45], the curvature is enhanced, underlining the predominant effect of differential expansion between the layers over differential expansion between the fiber and matrix on actuation.

The initial state observed after printing is radically different between the two biocomposites. While cFF/PLA evidences a flat shape after printing (Fig. 3.c) showing a near zero stress state, cFF/PBS already has a curvature in the opposite direction to the curvature that is induced by moisture (Fig. 1.c).

This may be due to the difference in glass transition temperature between PLA and PBS (Tg_{PLA} = 56 °C and Tg_{PBS} = -28 °C) and also the crystallinity ratio that explains the different thermal stress states. The difference in curvature between the initial state (after printing) and zero-curvature state of the cFF/PBS accounts for about 15% of their total curvature variation and is due to a combination of thermal stress release and hygroscopic stresses. Further work needs to be done to decorrelate their contribution.

The reactivity of cFF/PLA and cFF/PBS, evaluated as the actuation kinetic (*i.e.,* the slope of the curvature curve as a function of time), is also drastically higher than for hygromorph biocomposites reinforced with short fibers for a similar reason as responsiveness [16]. The cFF/PBS exhibits a 6-fold higher reactivity than composites based on the PLA matrix (Table 3). Reducing the constraining effect of the matrix on the fiber improves transient and stationary sorption by increasing the free volume of the polymer [48]. In addition, PBS (M = 0.9% at 20 °C) is more sensitive to moisture than PLA (M = 0.3% at 20 °C) [49,50].

After sorption and desorption, the hygromorph biocomposites do not return to their initial position. The cFF/PLA and cFF/PBS lose 51% and 30% of their actuation amplitude, respectively (Table 3). This concern was also observed for thermally compressed cFF/PP HBC [51], 4D-printed short-wood-fibers/PLA-PHA blend HBC [16] and wood/PLA-PHA blend with additional PA layers [52]. Several explanations are proposed, such as high internal stresses in the

Table 2
Mechanical, hygroscopic and actuation properties of cFF/PLA and cFF/PBS HBC.

Materials	Longitudinal Modulus E_1 (GPa)	Transverse modulus (MPa)	Anisotropic ratio (n = Ep/Ea)	$\beta_T.\Delta M_\infty$ (%)	Responsiveness (10^{-3} mm^{-1})	Reactivity (10^{-4} mm^{-1} min^{-1})
cFF/PLA	15.6 ± 2.2	2.5 ± 0.1	6.24	1.26 ± 0.5	27.5 ± 2.0	1.2 ± 0.4
cFF/PBS	10.3 ± 0.7	0.43 ± 0.04	24	3.8 ± 0.4	54.7 ± 3.0	7.2 ± 0.9

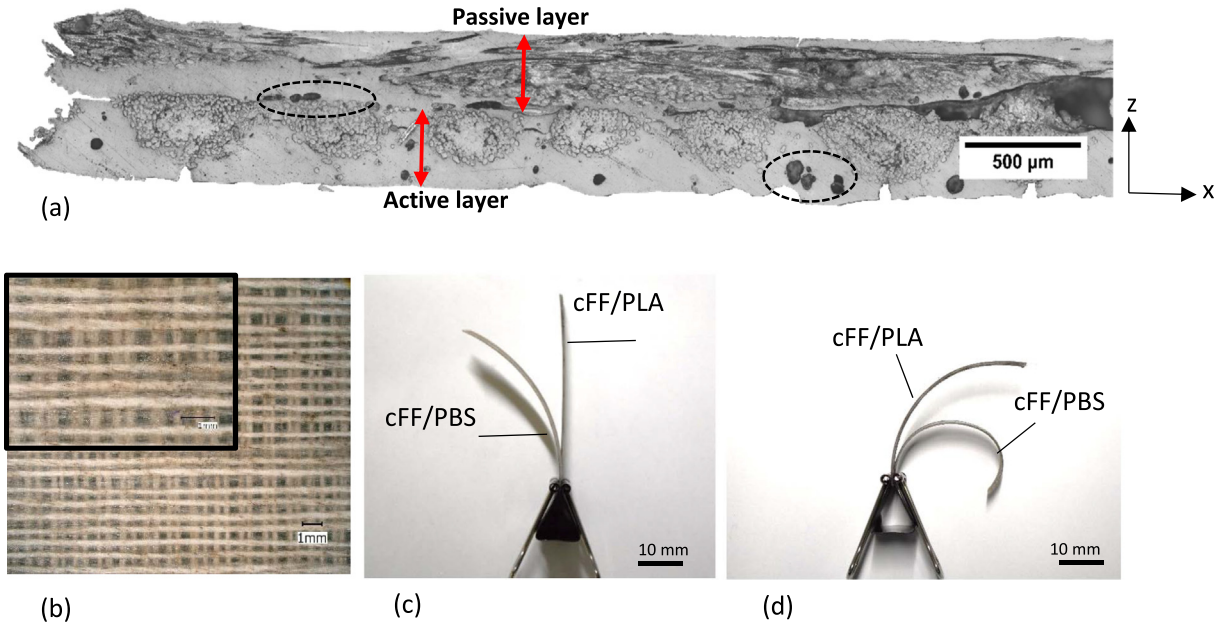

Fig. 1. Microscopic observation of a cFF/PLA cross section showing bilayer microstructure and interlaminar defects (a), in-plane microstructure with a higher magnification insert showing local misalignment and variation of interfilament distance (b), comparison of the initial state of the hygromorphic biocomposites cFF/PLA and cFF/PBS taken after printing (c) and after immersion in water (d).

Table 3
The ratio m, the ratio of each layer height, the overall compression ratio and the responsiveness of cFF/PLA Hygromorph BioComposites. The basic printing sequence is [90/0°]. * means a printing sequence of [0/90°].

Theoretical 90° and 0° Layer Height (mm / mm)	$m_{theoretical\ ratio}$	Total thickness (µm)	Passive layer thickness (µm)	Active layer thickness (µm)	$m_{real\ ratio}$	Compression ratio (-)	Responsiveness (10^{-3} mm^{-1})
0.2 / 0.2	1	562 ± 17	269 ± 24	310 ± 12	0.83 ± 0.02	1.80	26.2 ± 3.0
0.3 / 0.3	1	602 ± 14	284 ± 12	316 ± 5	0.90 ± 0.04	1.66	27.5 ± 2.0
0.4 / 0.4	1	719 ± 13	400 ± 12	335 ± 5	1.19 ± 0.02	1.40	15.3 ± 1.0
0.2 / 0.1	0.5	553 ± 34	281 ± 33	296 ± 21	0.93 ± 0.06	1.80	15.3 ± 2.0
0.2 / 0.4	2	651 ± 18	354 ± 22	306 ± 16	1.15 ± 0.07	1.54	13.2 ± 1.0
0.2 / 0.2 *	1	598 ± 44	293 ± 23	300 ± 14	0.98 ± 0.06	1.70	10.0 ± 2.0

transverse direction that may overcome the transverse tensile strength and promote crack propagation [53]. Indeed, the higher the moisture gradient, the greater the internal hygroscopic stresses [54]. These immersion tests represent a severe environment that can trigger an additional degradation mechanism through leaching of pectin-based polysaccharides as well as hornification, *i.e.,* the reconfiguration of cellulose that occurs after the wet/dry cycle and leads to an irreversible loss of fiber sensitivity to water and thus swelling ability [20,52,56]. Improved actuation reliability has been evidenced by grafting the matrix with a coupling agent [51], using unidirectional fiber tapes with untwisted fiber bundles to promote interfacial load transfer capability [56] and selecting moisture-resistant fibers such as jute [20].

Finally, matrix stiffness is a key criterion that reinforces the hygromorph feature of the continuous natural fiber, which is currently technically limited by the fiber fraction. This confirms the superiority of 4D-printed hygromorphic biocomposites with continuous fibers and especially cFF/PBS over current discontinuous fibers-based HBC and wood bilayer hygromorphs for their customized performance.

3.2. Effect of design and slicing parameters on actuation

3.2.1. Variation of layer height to control thickness and stiffness ratio

To design the hygromorph biocomposites, the analytical solution given by Timoshenko [57] of the curvature variation Δk of a beam subjected to bending due to the difference $\Delta\beta$ of the hygroscopic expansion coefficients and the moisture content ΔC is selected.

$$\Delta k = \frac{\Delta\beta \Delta C f(m,n)}{h} \tag{3}$$

$$f(m,n) = \frac{6(1+m)^2}{3(1+m)^2 + (1+mn)\left(m^2 + \frac{1}{mn}\right)} \tag{4}$$

In (Eq (3)) and (Eq (4)), $m = t_p/t_a$, where t_p and t_a represent the passive layer and the active layer thicknesses, respectively. The parameter n is equal to E_p/E_a, where E_p and E_a represent the longitudinal modulus of the passive and active layers, respectively. The differential hygroscopic expansion between the active β_a and passive β_p layer is represented by $\Delta\beta$. The difference in water content between the immersion and drying steps is ΔC.

To achieve the greatest curvature, the total thickness of the bilayer sample should be kept as small as possible to reduce the bending stiffness. Therefore, the minimum number of layers was selected, namely two layers.

Then, an optimal thickness ratio $m = \frac{t_p}{t_a}$ corresponding to the highest value of curvature should be found (Fig. 2.a).

The specificity of 4D printing compared to the conventional process is the ability to locally modify the *m*-ratio through the compression ratio between layers or even within a layer thanks to the "Layer Height" (LH) parameter (Fig. 3). However, the control

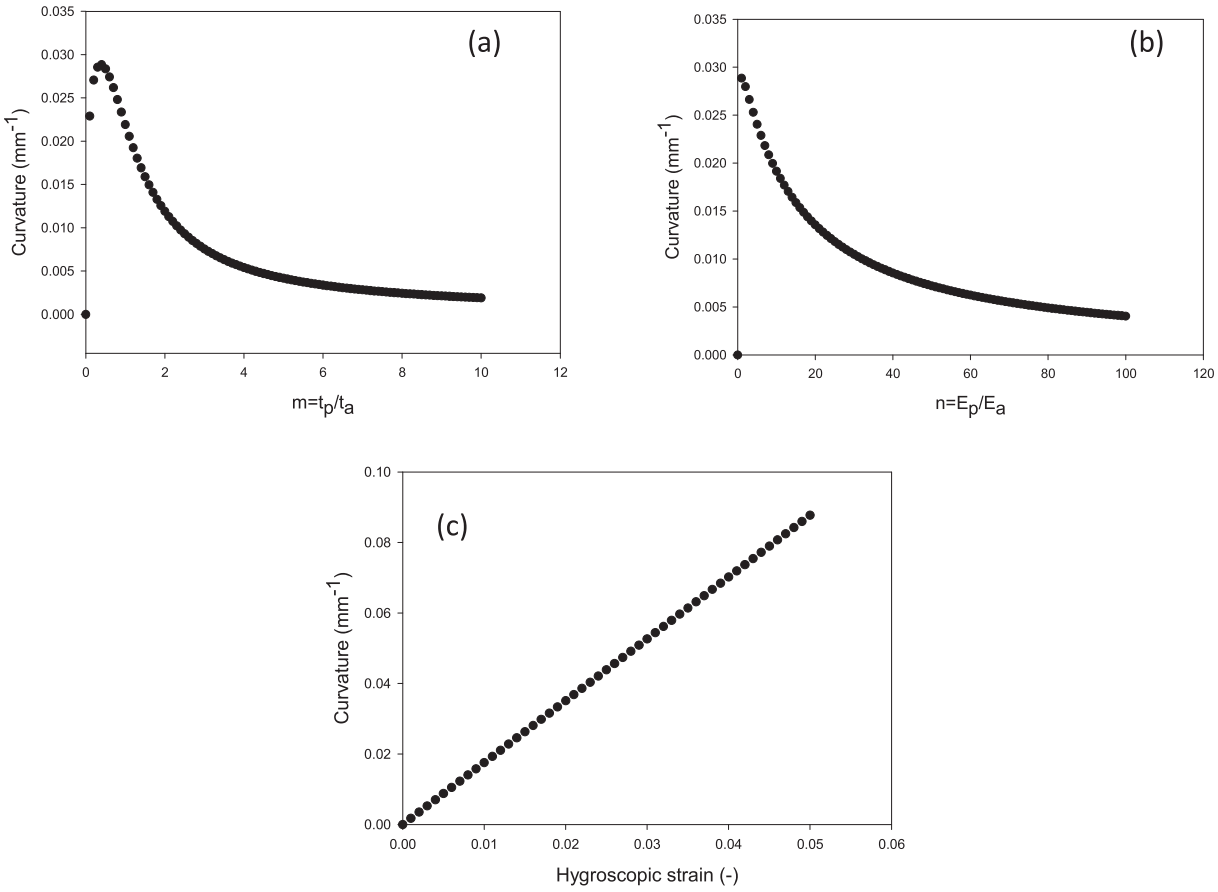

Fig. 2. Evolution curvature as a function of m ratio (t_p/t_a) with n = 7.05 (a), n ratio (E_p/E_a) with m = 1 (b) and hygroscopic strain with n = 7.05 and m = 1 (c) for cFF/PLA hygromorph biocomposites.

of the *m-ratio* with continuous flax fibre HBC is not straightforward.

Indeed, the total thickness presents differences with the predefined Layer Height depending on the selected LH values (Table 1). Thus, even if a similar LH is maintained between the first and second layer, a balanced *m* ratio of 1 is difficult to achieve. Thus, the *m ratio* varies from 0.87 to 1.19 with an increase in LH from 0.2 to 0.4 mm. The best match between the theoretical and measured *m ratio* is observed for a Layer Height of 0.3 mm. Actually, printing a layer causes a warming effect on the underlying layer, which can lead to a reduction in polymer viscosity and better compaction of the first layer. This is of great importance when a small number of layers are printed, as in the case of the current HBC. In addition, it has been shown that the architecture of the yarn involves three regimes during printing, namely over-compaction, compaction and under-compaction [32]. A threshold was observed around LH = 0.3 mm, which explains the better correspondence between the theoretical and experimental *m ratio*. Thus, programming a Layer Height of less than 0.3 mm always leads to an over-compaction and a layer thickness of approximately 0.2–0.25 mm. Increasing LH towards under-compaction (LH = 0.4 mm) decreases the compression ratio from 1.8 to 1.4 and increases the porosity content.

Then, changing the printing sequence from [90/0°] to [0/90°] ((0.2 / 0.2)) modifies the *m* ratio from 0.87 to 0.98. This is likely due to a higher Trip Number (TN) for a transversally printed layer compared to a longitudinal layer, that leads to a larger layer thickness [32]. Consequently, when 4D printing with [90/0°] stacking, the second layer is more compressed than when printing with [0/0°] stacking sequence.

Thus, understanding the potential calibration of LH allows for a wide variety of *m ratio*s that directly influence HBC responsiveness. Therefore, applying a theoretical *m ratio* of 1 induced HBC responsiveness from 10 to 27.5 mm^{-1} (Table 3). Another possibility of 4D printing is to change the LH between the first and second layer. This change modifies the m ratio from 0.87 to 1.16 and almost doubles the responsiveness from 13.2 to 26.2 mm^{-1}.

The LH parameter influences the stiffness of each layer, with EL_1 varying from 17.2 to 12.1 GPa for LH = 0.4 [32]. Therefore, LH also influences the *n ratio* in the Timoschenko's equation. The latter states that an increase in the *n* ratio leads to a reduction in the curvature (Figure .b). 4D printing should allow us to reduce the passive layer tensile moduli while keeping the active layer moduli high.

LH has also an effect on the porosity of cFF/PLA biocomposites, which follows an exponential increase with Layer Height from (porosity volume fraction, Vp) Vp = 2 ± 0.6% for a layer height of 0.2 mm to 17.6 ± 3.9% for a layer height of 0.6 mm. Previous work has evidenced that the porosity content has a negative effect on the hygroscopic expansion of 3D printed biocomposites [16], while the curvature of the HBC changes linearly with hygroscopic expansion (Fig. 2c).

Finally, LH is a complex slicing parameter that influences all parameters of the Timoschenko equation *n, m and* $\Delta\beta.\Delta C$ and provides the opportunity to locally determine the Hygromorph biocomposite responsiveness accurately. For example, Fig. 4 presents a schematic drawing of proposed linear distribution of LH in the passive layer (LH_p) from LH_p = 0.1 to 0.6 mm which control locally the m and n ratio. The corresponding printed sample is presented in Fig. 4b and exhibit a discontinuous curvature (along

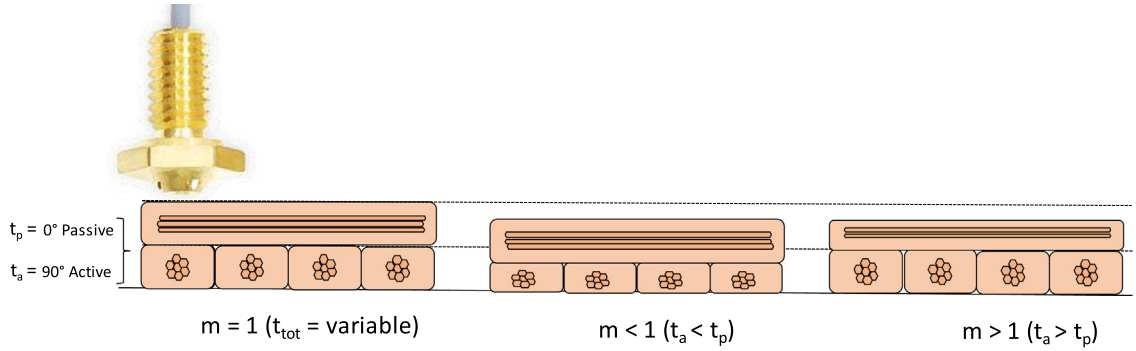

Fig. 3. Schematic view of the concept of different compression ratios allowing a multiple combination of the m ratio with only two printed layers. t_{tot} is the total thickness of the laminate, t_a and t_p are the thickness of the active and passive layers respectively.

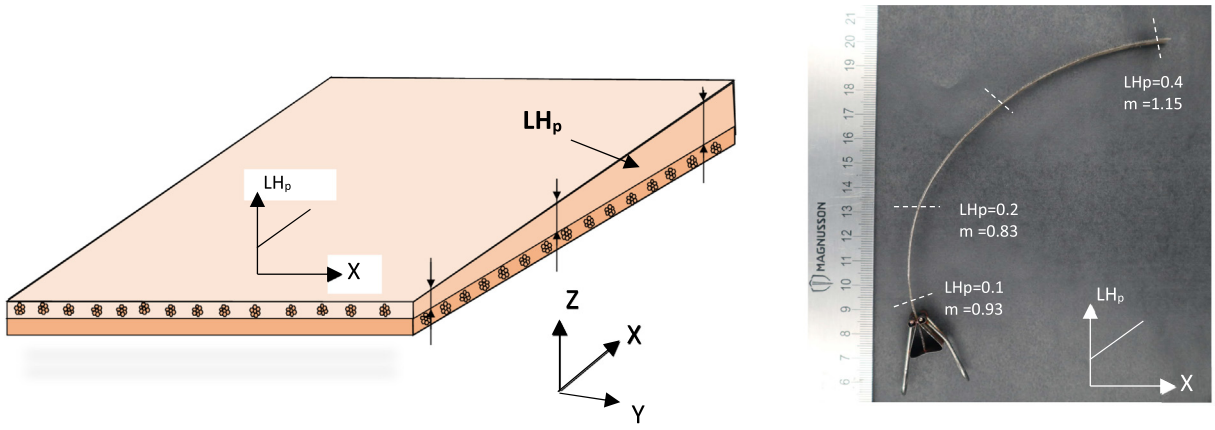

Fig. 4. Schematic drawing of the HBC showing an example of evolution of the Layer Height in the passive layer (LHp) (a); Layer Height in the active layer is constant. Printed sample with LH_p varying linearly from 0.1 to 0.6 (b).

the length) representing locally the m ratio and the corresponding curvature data presented in Table 3.

3.2.2. Interfilament distance to control stiffness ratio

As highlighted by Timoschenko equations, the ratio n (E_p/E_a) is a key parameter to control the responsiveness of bilayer actuators. Decreasing the n ratio improves the curvature as previously mentioned. To decrease the ratio n, *either reduce* E_p or increase E_a. (The subscripts "a" and "p" stand for active and passive respectively). Controlling the stiffness of composite laminates can generally be accomplished by microscale adjustments to the component selection, fiber content or orientation. Unlike conventional manufacturing processes, additive manufacturing such as FFF offers a new dimension by customizing the mesoscale architecture of materials (ply scale) and their related properties. The distance between filaments influences the in-plane stiffness of a continuous-flax reinforced biocomposite by changing the amount of material in the sample volume [32].

Fig. 5a shows a schematic diagram of the Hygromorph BioComposite composed of two layers, where the active and passive layers have different interfilament distance (ID_a = 0.6 mm and ID_p = 3 mm,) and the curvature in the x-axis is targeted thanks to the slender geometry (Length ≫ Width). Fig. 4b shows micrograph images of cFF/PBS hygromorph biocomposites with the passive layer having different ID_p from 0.6 to 6 mm, and a constant ID_a of 0.6 mm. The choice of changing the interfilament distance on the active or passive layer greatly affects the actuation behavior of the HBC, not only the amplitude of curvature but also the direction of actuation. Indeed, if one considers that the targeted curvature is along the x-axis and provides that the transverse expansion of the active layer is foreseen, a change in the spatial distribution of filament within the passive layer is envisaged (Fig. 5b).

Changing ID_a while keeping ID_p constant leads to the opposite result, as increasing interfilament distance reduces the hygroexpansion of a hygromorphic composite [15]. In addition, based on a balanced asymmetric laminate and depending on the slenderness of the sample, the transverse swelling of the passive layer can exceed the transverse swelling of the active layer and lead to an opposite curvature (not shown here). This point deserves to be further investigated in future work as it opens the door to new multidirectional actuation.

Thus, an increase of ID_p from 0.6 to 6 mm will more than double the responsiveness of the HBC (Fig. 6a). Varying the interfilament distance opens up the design envelope of the 4D-printed HBC considerably. This is corroborated by several realizations on different systems. For example, on an actuation system opposite to HBC, *i.e.,* with a reactive matrix and a passive fiber, Wang et al. [26] evidenced a 25% thermally induced curvature change on the carbon/PA bilayer when the distance between the filaments varies from 2 to 12 mm. Gladman et al. [15] observed a similar phenomenon in their hydrogel/cellulose nanofibrils systems. They stated that since a fixed volume of material is considered, an effective thickness can be given by the volume of material divided by the cross-sectional area. The effective thickness is then used in the calculation of bending stiffness. The interfilament distance *ID* also plays a major role on the reactivity of cFF/PBS HBC with a 300% increase in the transient mechanism with ID_p increasing from 0.6 to 6 mm (Fig. 6.b). It is important to note that the standard devia-

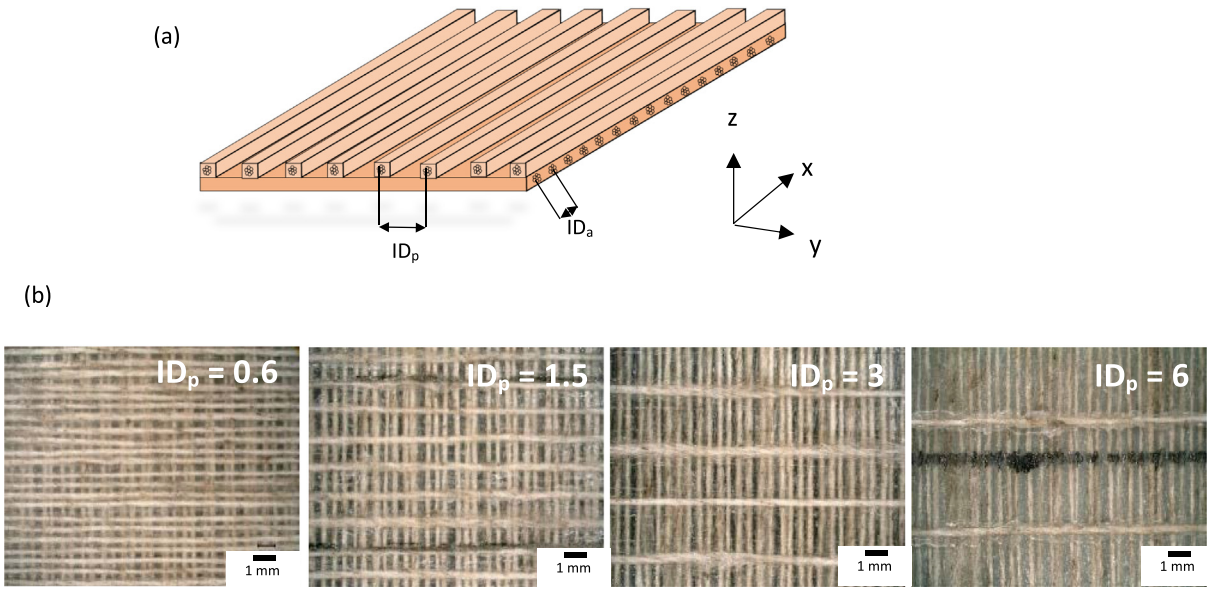

Fig. 5. Schematic drawing of the HBC showing the interfilament parameters ID_p and ID_a for the passive and active layers respectively (a), micrograph pictures of the mesoscale architecture of cFF/PBS as a function of the interfilament distance in the passive layer ID_p (b). Subscripts "a" and "p" stand for active and passive, respectively).

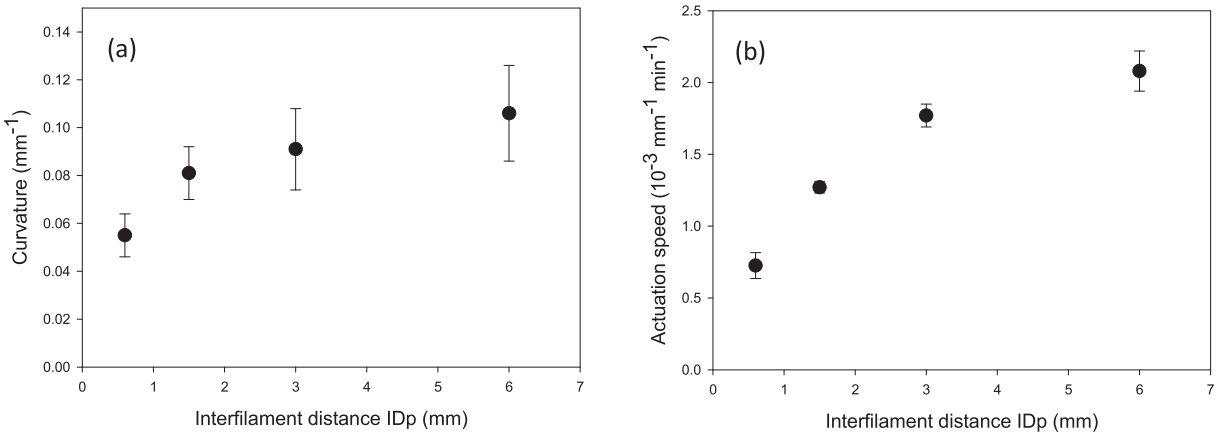

Fig. 6. Evolution of curvature actuation (a), actuation speed (b) as a function of interfilament distance (IDp) for cFF/PBS HBC.

tion increases with increasing ID_p. This may be due to the effect of potential misalignment of the yarn due to a lack of neighboring yarn, but also due to the increase in the polymer flow area of the previous layer that may change the local thickness ratio (see Fig. 7b).

The open voids left by the distance between the filaments increase the surface-to-volume ratio of the sample and thus make the material more accessible to interactions with moisture. This could be compared to the vascular capacity of wood tissue, which promotes moisture exchange through controlled cellular architecture [27]. This strategy has already been successfully used in holed hydrogel bilayers actuators [58] and milled-in grooves on a wood bilayer [59] to accelerate the response. Interestingly, the ability to design HBCs with different reactivity by controlling the architecture can transform a simple HBC actuation into a complex sequential actuation allowing the morphing of complex structures. The different actuation time scales embedded into the HBC architecture will allow a non-uniform response to a uniform stimulus.

The reliability of these 4D-printed cFF/PBS also depends on the interfilament distance (ID). A higher ID_p reduces the ability of the HBC to be fully reversible even though stabilization around 40% of the mechanism is observed above 3 mm (Fig. 7a). As already discussed, the degradation induced by water immersion is severe but the increase in ID_p leads to a greater reduction which should be due to the reduction of the interfacial area (fiber/matrix and interlaminar areas) to transfer the loads. Printing cFF/PBS HBC with orthogonally oriented layers leads to a complex bonding area. Fig. 7.b shows that due to the lack of neighboring filaments in the passive layer, the flowing area of the polymer of the previous layer is larger. This point was discussed elsewhere [32]. This may affect local stress state and should be studied further in the future.

3.2.3. Gradual and local variation of the stiffness to complexify morphing

Instead of printing the passive layer with a constant interfilament distance, it is possible to complexify the spatial distribution of the flax yarns to achieve variable composite stiffness [60] (in-plane gradient of stiffness). Therefore, the microstructure provided by additive manufacturing allows for a spatial and therefore temporal distribution of actuation within the same material, similar to biological structure (e.g., pine cone [27]). Fig. 8.a shows the different distributions of flax yarns in the passive layer of a cFF/PBS

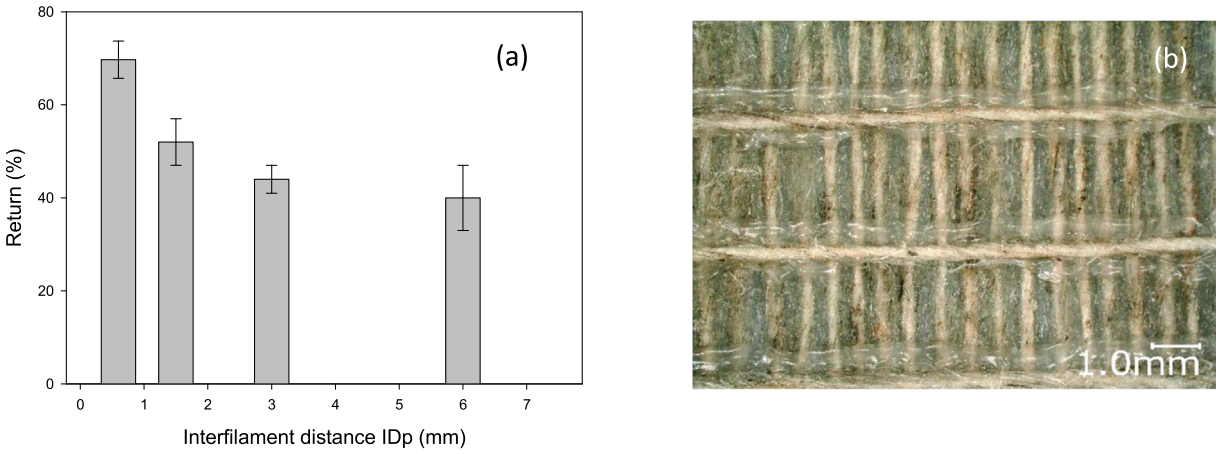

Fig. 7. Evolution of the position of cFF/PBS HBC after one sorption/desorption cycle as a function of interfilament distance, ID_p (a). In-plane observation of cFF/PBS HBC with ID_p = 3 mm showing the interfacial and interlaminar regions (b).

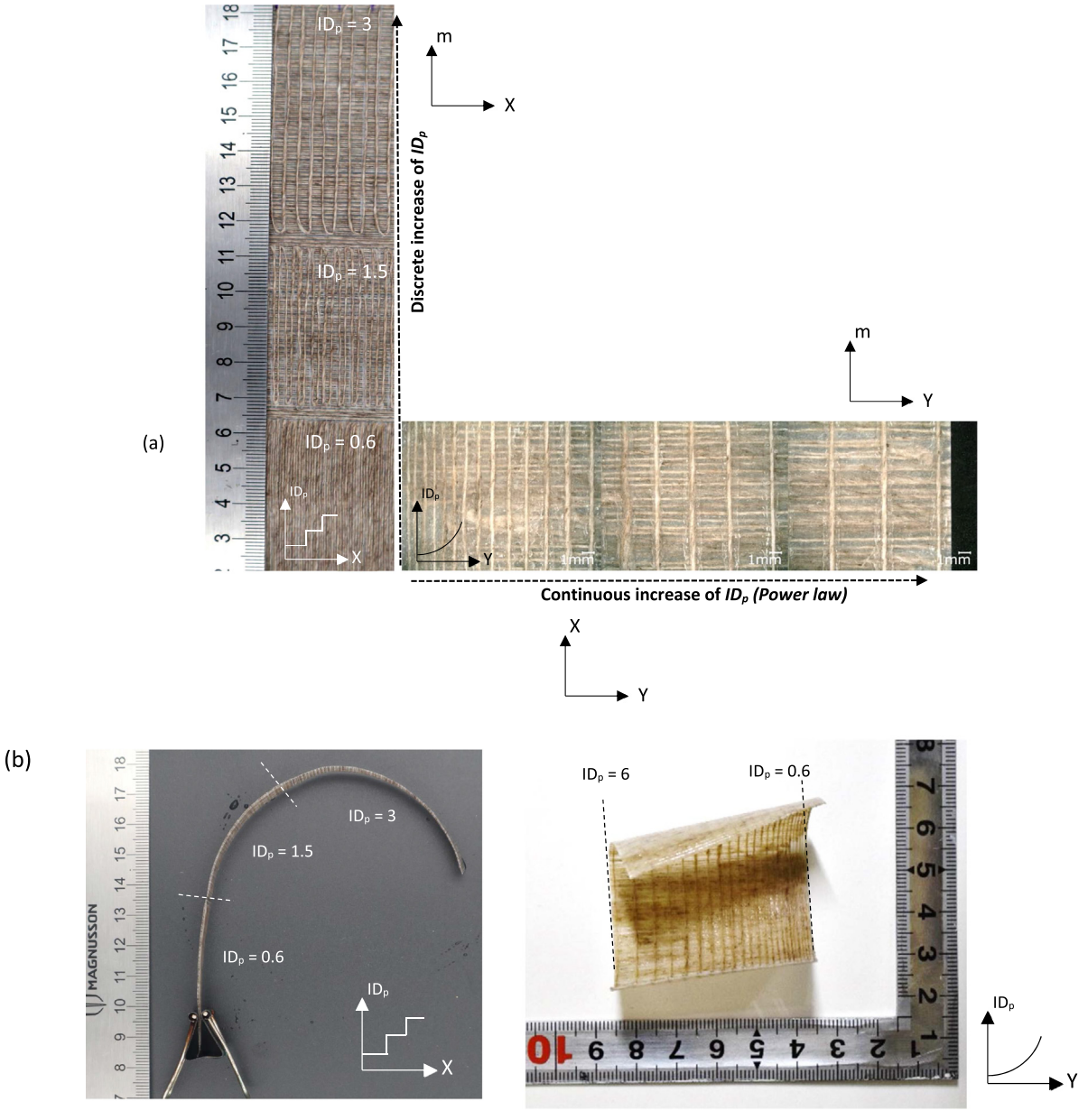

Fig. 8. Discrete and continuous (power law) distribution of Interfilament distance within the passive layer of cFF/PBS HBC and its response to immersion in water (a) showing a gradual response of the surface along the X or Y direction (b).

HBC in the longitudinal (X direction) and transverse direction (Y direction) for two different samples. A discrete distribution of the flax yarn along line X is proposed with three compartments (ID_p = 0.6; 1.5 and 3 mm) while along line Y, a continuous distribution of the flax yarn following a power law function is applied.

Since an increase in ID_p implies an increase in curvature responsiveness and reactivity (Fig. 6.a and b), samples printed with a gradual *IDp* distribution have a complex motion geometry with gradual curvature along its length or width (Fig. 8a and b), from edge to edge and a sequential time evolution.

Providing the encouraging ability of 4D printing to control the in-plane mesostructure of the laminate, cFF/Polymer HBC can achieve a non-uniform curvature. Generally speaking, the concept of gradual in-plane actuation could withstand a reconfigurable surface. Momeni et al. [61] proposed smart wind turbine blades mimicking plant leaves, whose gradual in-plane curvature allows for aeroelasticity adaptation.

3.2.4. Programming of local heterogeneities within the HBC

Programming the spatial distribution of the flax yarn can be combined with the heterogeneities to yield predefined and accurate results [62]. An asymmetrical lay-up results in a curvature induced by the differential hygro-expansion between the active and passive layers. The creation of a localized area can be designed in different ways: a localized bilayer zone where the rigid links consists of only one layer of material or a balanced trilayer with a gap leaving a free curvature. As HBCs are anisotropic materials, upon actuation, the rigid link consisting of a single biocomposite layer will be constrained by the bilayer and out-of-plane bending will be generated (not shown here). Thus, the second solution is adopted. Fig. 9a shows a schematic view of the hinge-like compliant mechanism designed and tested here. The parameter *a* represents the hinge gap, the area where the bilayer can actuate.

The orientation of the flax yarn is similar to those evaluated previously, [0/90°]. This area has been considered elsewhere as a "valley" or "mountain" fold line for designing complex adaptive origami structures [63]. Fig. 9a and b show a schematic view and printed HBC samples of an example of the result obtained for a 20 mm long hinge. Compared to a simple bilayer (Fig. 6.b and c), the actuation motion provided by the compliant hinge is clearly localized, enabling better control of the final shape (Fig. 9b). Thus, the actuation curvature becomes an actuation angle. Modifying the hinge length from 10 to 30 mm doubles the actuation angle for a sample where ID_p is 0.6 mm (Fig. 10.a).

For comparison, the equivalent actuation angle of the entire bilayer sample (70 mm) is plotted on the same graph (Fig. 10.a). The design of a compliant hinge system reduces the total movement of the bilayer due to the constraining effect of the rigid links and the reduction of the bending moment. This has already been observed with SMP smart hinges [64] or hydrogel trilayer hinges [63]. Based on the previous section which focuses on the effect of the interfilament distance, the compliant hinge pattern was optimized.

By increasing ID_p, the interfilament distance in the passive layer of the bilayer implies a drastic increase of the actuation angle by a factor of 2 for a similar hinge length.

Hence, the combination of hinge gap and interfilament distance create a dedicated spatial pattern that allows for better control of the architecture of the 4D-printed HBC and, consequently, expands their potential through precise actuation. Going further, Zolfagharian et al. [37] showed on a PS/Chitosan hydrogel actuator whose complex hinge pattern by printed square, honeycomb and zigzag paths can open the design window. Further investigation dedicated to HBC should be carried out in this direction.

After drying, the sample with a hinge gap of 10 to 30 mm and the full sample (70 mm) exhibit a curvature of 85 to 70% of their initial position. Again, increasing ID_p reduces reliability with only 30% return capacity.

The actuation speed is changed according to the hinge gap. Increasing the hinge gap from 10 to 30 mm can double the response speed, although it is still drastically lower than for the full 70 mm long sample. A change in the hygroscopic stress state within the sample could be argued.

Similarly, according to the results shown in Fig. 10.b, increasing the interfilament distance can speed up the actuation by more than 300%. The potential for designing compliant hinges with a wide range of temporal responses is evidenced, paving the way for multi sequential folding structures.

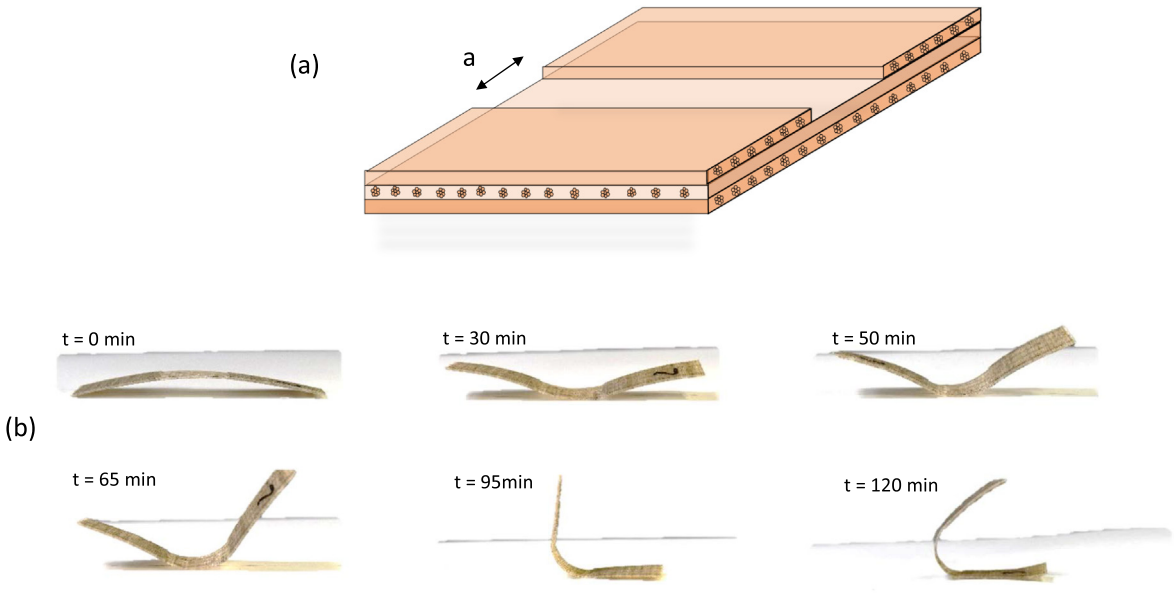

Fig. 9. Schematic view of the compliant hinge-like mechanism made of cFF/PBS. Parameter a represents the hinge gap where the actuation is located (a). Photograph of the cFF/PBS during actuation (a = 20 mm and ID_p = 3 mm) (b).

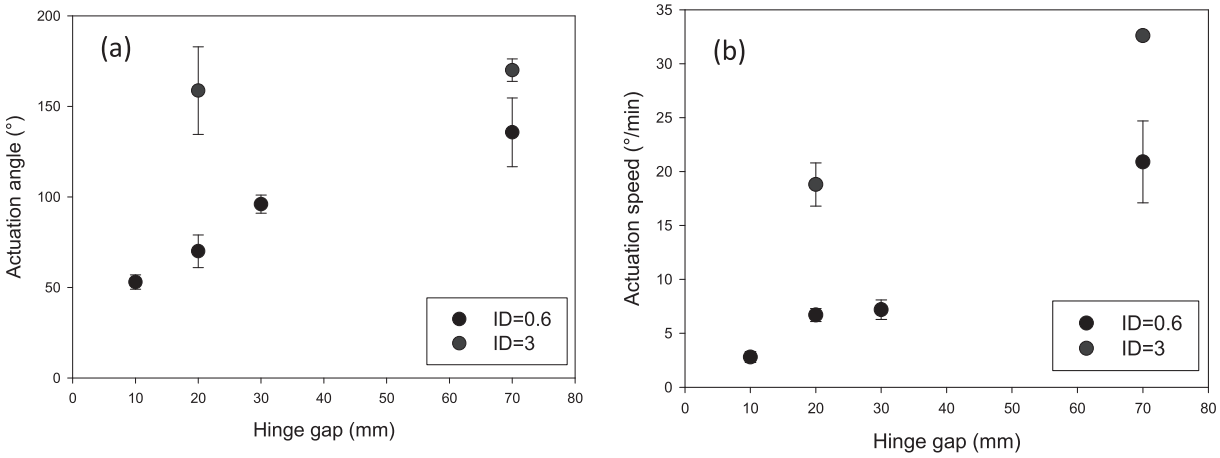

Fig. 10. Evolution of actuation angle (a) and speed (b) as a function of hinge gap for different cFF/PBS HBC interfilament spacings.

4. Conclusion

4D-printing of shape-changing materials rarely focuses on natural fibre composites and even less on continuous fiber composites, although they offer better elastic properties and an anisotropy control.

This work has the novelty of tailoring 4D printing to HBC, opening the way to the design of a sophisticated 4D printed HBC metamaterial with a sequential response. Hygromorph BioComposites (HBC) based on continuous flax fiber with biobased and biodegradable matrices (PLA and PBS) and bioinspired microstructures have been proposed.

Unlike most of the available research on on–the-shelf materials, the present work aimed to take advantage of the customized HBC to provide higher hygroscopic expansion and actuation. Material selection has been discussed through characterization of hygroelastic properties with contrasting stiffness of the polymer matrices: E_{PLA} = 3.6 GPa and E_{PBS} = 0.64 GPa. These two materials allow HBCs to overcome the mechanical, hygroscopic and actuating properties of short-natural-fiber based hygromorphic biocomposites. A great improvement in actuation potential with + 98% responsiveness, + 500% of reactivity was observed for PBS-based HBC compared to PLA-based counterparts. Thus, a lower stiffness reduces internal stresses and the constraining effect of the matrix on the fibres, and allows hygroexpansion of the fibers. Therefore, matrix selection can compensate for the low fiber content, a limitation encountered in the 4D printing process.

The design of HBC can be achieved by following the Timoschenko's model. Each parameter was discussed in the context of 4D printing. The ratio *m* describing the ratio between the thickness of the passive layer and the active layer shows an optimum leading to the highest curvature. 4D printing enables this ratio to be locally changed by controlling the Layer Height parameter (LH) within a layer or between multiple layers independently. However, due to the compressibility of flax yarn inside the filament, the *m ratio* was not easy to control although, interestingly, it can be changed over a wide range.

LH also influenced the stiffness of each layer and therefore influenced the *n ratio* of the modified Timoschenko's equations. LH has also an effect on the porosity content win cFF/PLA biocomposites which has been previously shown to have a negative effect on the hygroscopic expansion of printed biocomposites.

Further work should be done to better understand the interdependence of all slicing parameters on actuation. Machine learning data treatment would be worth using in the future.

Unlike conventionally manufactured composite laminates, where stiffness can be barely adjusted in the in-plane direction, additive manufacturing offers a new dimension by customizing the mesoscale architecture of materials and their related properties. Thus, the Interfilament Distance (ID) influences the in-plane-stiffness of a continuous-flax reinforced biocomposite by changing the amount of material in the sample volume. Increasing this parameter from 0.6 to 6 mm improved both the amplitude (+92%) and speed of actuation (+186%) by reducing the bending modulus and providing a higher surface-to-volume ratio for moisture sorption.

Controlling actuation kinetics with the same material, but with a different architecture, paves the way for HBC design for complex morphing and multi-step shape changing materials. Further work should be done on combining the relationship between mesostructure, overall geometrical effect and subsequent actuation potential.

CRediT authorship contribution statement

A. Le Duigou: Supervision, Methodology, Writing – review & editing. **T Fruleux:** Investigation. **R. Matsuzaki:** Writing – review & editing. **G. Chabaud:** Investigation. **M. Ueda:** Writing – review & editing. **M. Castro:** Writing – review & editing.

Declaration of Competing Interest

The authors declare that they have no known competing financial interests or personal relationships that could have appeared to influence the work reported in this paper.

Acknowledgments

The authors wish to acknowledge "Isblue (https://www.isblue.fr/fr/)" and CNRS AAP MITI BIOMIMETISME for financial support.

Data availability

The datasets generated during and/or analysed during the current study are available from the corresponding author on reasonable request.

References

[1] S. Tibitts, The emergence of 4D printing, TED talks (2013).
[2] Q. Ge, H. J. Qi, M.L. Dunn, Active materials by four-dimension printing, Appl. Phys. Lett., vol. 103, no. 13, 2013.
[3] E. Pei, 4D printing: dawn of an emerging technology cycle, Assem. Autom. 34 (4) (2014) 310–314.
[4] A. Zolfagharian, A. Kaynak, A. Kouzani, Closed-loop 4D-printed soft robots, Mater. Des. 188 (2020) 108411.

[5] M. Bodaghi, A.R. Damanpack, W.H. Liao, Adaptive metamaterials by functionally graded 4D printing, Mater. Des. 135 (2017) 26–36.
[6] S. Miao, N. Castro, M. Nowicki, L. Xia, H. Cui, X. Zhou, W. Zhu, S.-J. Lee, K. Sarkar, G. Vozzi, Y. Tabata, J. Fisher, L.G. Zhang, 4D printing of polymeric materials for tissue and organ regeneration, Mater. today 20 (10) (2017) 577–591.
[7] T. Van Manen, S. Janbaz, and A. Zadpoor, "Programming 2D/3D shape-shifting with hobbyist 3D printers," Mater. Horiz., vol. 4, no. 1064, 2017.
[8] M. Bodagh, R. Norooz, A. Zolfagharian, M. Fotouhi, S. Norouzi, 4D printing self-morphing structures, Materials (Basel) 12 (8) (2019) 1353.
[9] T. Van Manen, S. Janbaz, K. Jansen, A. Zadpoor, enables flat constructs to fold themselves into geometrically-complex 3D objects, Nat. Portf. (2021).
[10] M. Bodaghi, W.H. Liao, 4D printed tunable mechanical metamaterials with shape memory operations, Smart Mater. Struct. 28 (2019) 045019.
[11] M. Bodaghi, A. Damanpack, W. Liao, Triple shape memory polymers by 4D printing, Smart Mater. Struct. 27 (2018) 065010.
[12] F. Momeni, S. M.Mehdi Hassani.N, X. Liu, J. Ni, A review of 4D printing, Mater. Des. 122 (2017) 42–79.
[13] J. Zhou, S. Sheiko, Reversible shape-shifting in polymeric materials, J. Polym. Sci. Part B Polym. Phys. 54 (14) (2016) 1365–1380.
[14] C. Yang, B. Wang, D. Li, X. Tian, Modelling and characterisation for the responsive performance of CF/PLA and CF/PEEK smart materials fabricated by 4D printing, Virtual Phys. Prototyp. 12 (1) (2017) 69–76.
[15] A. Sydney Gladman, E.A. Matsumoto, R.G. Nuzzo, L. Mahadevan, J.A. Lewis, Biomimetic 4D printing, Nat. Mater. 15 (4) (2016) 413–418.
[16] A. Le Duigou, M. Castro, R. Bevan, N. Martin, 3D printing of wood fibre biocomposites: From mechanical to actuation functionality, Mater. Des. 96 (2016) 106–114.
[17] E. Vazquez, C. Randall, J. Duarte, Shape-Changing Architectural Skins a Review on Materials, Design and Fabrication Strategies and Performance Analysis, J. Facade Des. Eng., vol. 7, no. 2, 2019.
[18] D. Correa, A. Menges, 3D Printed Hygroscopic Programmable Material Systems, MRS Online Proceeding Libr. Arch., vol. 1800, no. DOI: 10.1557/opl.2015.644, 2015.
[19] A. Le Duigou, P. Davies, C. Baley, Replacement of Glass / Unsaturated Polyester Composites by Flax / PLLA Biocomposites : Is It Justified ? no. December, 2011.
[20] A Le Duigou, S Requile, J Beaugrand, F Scarpa, M Castro, Natural fibres actuators for smart bio-inspired hygromorph biocomposites, Smart Mater. Struct., vol. 26, no. 12, 2017.
[21] T. Cheng et al., Bio-inspired motion mechanisms: computational design and material programming of self-adjusting 4D-printed wearable systems, Adv. Sci. 8 (13) (2021) 2100411.
[22] I. Burgert, P. Fratzl, Actuation systems in plants as prototypes for bioinspired devices, Philos. Trans. A. Math. Phys. Eng. Sci. 367 (1893) (2009) 1541–1557.
[23] R. Kay, K. Nitièma, D. Correa, The Bio-inspired Design of a Self-propelling Robot Driven by Changes in Humidity, Proc. 38th eCAADe, vol. 2, 2020.
[24] D. Correa et al., 3D printing wood :Programming hygroscopic material transformations, 3D Print. Addit. Manuf., vol. 2, no. 3, pp. 106–116, 2105.
[25] A. Le Duigou, M. Castro, Evaluation of force generation mechanisms in natural, passive hydraulic actuators, Sci. Rep., vol. 18105, no. doi: 10.1038/srep18105, 2016.
[26] Q. Wang, X. Tian, L. Huang, D. Li, A.V. Malakhov, A.N. Polilov, Programmable morphing composites with embedded continuous fibers by 4D printing, Mater. Des. 155 (2018) 404–413.
[27] D. Correa et al., 4D pine scale: biomimetic 4D printed autonomous scale and flap structures capable of multi-phase movement, Philos. Trans. A. Math. Phys. Eng. Sci. 378 (2167) (2020) 20190445.
[28] A. Le Duigou, D. Correa, M. Ueda, R. Matsuzaki, M. Castro, A review of 3D and 4D printing of natural fibre biocomposites, Mater. Des. 194 (2020) 108911.
[29] R. M. Erb, J. S. Sander, R. Grisch, A.R. Studart, Self-shaping composites with programmable bioinspired microstructures, Nature, pp. 1–8, 2013.
[30] A. Le Duigou, G. Chabaud, F. Scarpa, M. Castro, Bioinspired electro-thermo-hygro reversible shape-changing materials by 4D printing, Adv. Funct. Mater. 1903280 (2019) 1–10.
[31] A. Le Duigou, A. Barbé, E. Guillou, M. Castro, 3D printing of continuous flax fibre reinforced biocomposite for structural applications, Mater. Des. 180 (2019) 107884.
[32] A. Le Duigou, G. Chabaud, R. Matsuzaki, and M. Castro, "Tailoring the mechanical properties of 3D-printed continuous flax/PLA biocomposites by controlling the slicing parameters," Comp Part B, vol. 203, no. 108474, 2020.
[33] G. Van Opdenbosch, D. Fritz-Popovski, W. Wagermaier, O. Paris, C. Zollfrank, Moisture-driven ceramic bilayer actuators from a biotemplating approach, Adv. Mater. 28 (2016) 5235–5240.
[34] Y. Liu, J. Genzer, M.D. Dickey, 2D or not 2D: shape programming polymer sheets, Prog. Polym. Sci 52 (2016) 79–106.
[35] S. Nam, E. Pei, A taxonomy of shape-changing behavior for 4D printed parts using shape-memory polymers, Prog. Addit. Manuf. 4 (2) (2019) 167–184.
[36] Y. Mao, K. Yu, M. Isakov, J. Wu, M. Dunn, H. Qi, Sequential self-folding structures by 3D printed digital shape memory polymers, Sci. Rep., vol. 5, no. 13616, 2015.
[37] A. Zolfagharian, A. Kaynak, S.Y. Khoo, A. Kouzani, Pattern-driven 4D printing, Sens. Actuat. A Phys. 274 (2018) 231–243.
[38] J. Baets, D. Plastria, J. Ivens, I. Verpoest, Determination of the optimal flax fibre preparation for use in unidirectional flax–epoxy composites, J. Reinf. Plast. Compos. 33 (5) (2014) 493–502.
[39] A. Le Duigou, A. Barbé, E. Guillou, M. Castro, 3D printing of continuous flax fibre reinforced biocomposites for structural applications, Mater. Des. (2019) 107884.
[40] D. Shah, Damage in biocomposites: Stiffness evolution of aligned plant fibre composites during monotonic and cyclic fatigue loading, Compos. Part A Appl. Sci. Manuf., Sep. 2015.
[41] Naturworks, IngeoTM Biopolymer 3260HP Technical Data Sheet, https://www.natureworksllc.com/~/media/Files/NatureWorks/Technical-Documents/Technical-Data-Sheets/TechnicalDataSheet_3260HP_injection-molding_pdf.pdf?la=en.
[42] A. Bourmaud, D. Åkesson, J. Beaugrand, A. Le Duigou, M. Skrifvars, C. Baley, Recycling of L-Poly-(lactide)-Poly-(butylene-succinate)-flax biocomposite, Polym. Degrad. Stab. 128 (2016) 77–88.
[43] A. Le Duigou, D. Correa, M. Ueda, R. Matsuzaki, M. Castro, A Review of 3D and 4D printing of natural fibres biocomposites, Mater. Des. 194 (2020) 108911.
[44] A. Le Duigou, V. Keryvin, J. Beaugrand, M. Pernes, F. Scarpa, M. Castro, Humidity responsive actuation of bioinspired Hygromorph BioComposites (HBC) for adaptive structures, Comp. Part A Appl. Sci. Manuf. 116 (2019) 36–45.
[45] A. le Duigou, J. Merotte, A. Bourmaud, P. Davies, K. Belhouli, C. Baley, Hygroscopic expansion: a key point to describe natural fibre/polymer matrix interface bond strength, Compos. Sci. Technol. 151 (2017) 228–233.
[46] P.P. Parlevliet, H.E.N. Bersee, A. Beukers, Residual stresses in thermoplastic composites—a study of the literature—Part II: Experimental techniques, Comp. Part A Appl. Sci. Manuf. 38 (3) (2007) 651–665.
[47] C. Baley, A. Kervoëlen, A. Le Duigou, C. Goudenhooft, A. Bourmaud, Is the low shear modulus of flax fibres an advantage for polymer reinforcement?, Mater Lett. 185 (2016) 534–536.
[48] M. Péron, A. Célino, Dine, M. Castro, F. Jacquemin, A. Le Duigou, "Study of hygroscopic stresses in asymetric biocomposite laminates," Compos. Sci. Technol., vol. 169, no. October 2018, pp. 7–15, 2019.
[49] A. Le Duigou, P. Davies, C. Baley, Seawater ageing of flax/poly(lactic acid) biocomposites, Polym. Degrad. Stab., vol. 94, no. 7, 2009.
[50] S. Charlon, N. Follain, J. Soulestin, M. Sclavons, S. Marais, Water Transport properties of poly(butylene succinate) and poly[(butylene succinate)-co-(butylene adipate)] nanocomposite films: influence of the water-assisted extrusion process, J. Phys. Chem. C 121 (1) (2017) 918–930.
[51] A. Le Duigou, M. Castro, Hygromorph BioComposites: effect of fibre content and interfacial strength on the actuation performances, Ind. Crops Prod. 99 (2017) 142–149.
[52] D. Correa, A. Papadopoulou, C. Guberan, N. Jhaveri, S. Reichert, A. Menges, S. Tibbits, 3D-printed wood: programming hygroscopic material transformations, 3D Print Addit. Manuf. 2 (3) (2015) 106–116.
[53] M. Péron, A. Célino, M. Castro, F. Jacquemin, A. Le Duigou, Study of hygroscopic stresses in asymmetric biocomposite laminates, Compos. Sci. Technol., 169 (2018) 7–15.
[54] M. Péron, A. Célino, F. Jacquemin, A. Le Duigou, Hygroscopic stresses in asymmetric biocomposite laminates submitted to various relative humidity conditions, Comp. Part A Appl. Sci. Manuf. 134 (2020) 105896, https://doi.org/10.1016/j.compositesa:2020.105896.
[55] A. Le Duigou, A. Bourmaud, C. Baley, In-situ evaluation of flax fibre degradation during water ageing, Ind. Crops Prod. 70 (2015) 204–210.
[56] J. Baets, D. Plastria, J. Ivens, I. Verpoest, Determination of the optimal flax fibre preparation for use in unidirectional flax-epoxy composites, J. Reinf. Plast. Compos. 33 (5) (2014) 493–502.
[57] S. Timoshenko, Analysis of bi-metal thermostats, J. Opt. Soc. Am. 11 (3) (1925) 233, https://doi.org/10.1364/JOSA.11.000233.
[58] G. Stoychev, L. Guiducci, S. Turcaud, J.W.C. Dunlop, L. Ionov, Hole programmed superfast multistep folding of hydrogel bilayers, Adv. Funct. Mater. 26 (42) (2016) 7733–7739.
[59] C. Vailati, P. Hass, I. Burgert, M. Ruggeberg, Upscaling of wood bilayers: design principles for controlling shape change and increasing moisture change rate, Mater. Struct. 50(250), 2017.
[60] K. Sugiyama et al., 3D printing of optimized composites with variable fiber volume fraction and stiffness using continuous fiber, Compos. Sci. Technol. 186 (2020) 107905.
[61] F. Momeni, S. Sabzpoushan, R. Valizadeh, M. Morad, X. Liu, J. Ni, Plant leaf-mimetic smart wind turbine blades by 4D printing, Renew. Energy, vol. 130, 2018.
[62] D. Raviv et al., Active printed materials for complex self-evolving deformations, Sci. Rep. 4 (7422) (2014) 1–8.
[63] A. Baker, S. Bates, T. Llewellyn-Jones, L. Valori, M. Dicker, R. Trask, 4D printing with robust thermoplastic polyurethane hydrogel-elastomer trilayers, Mater. Des. 167 (2019) 107544.
[64] S. Akbari, A.H. Sakhaei, K. Kowsari, B. Yang, A. Serjouei, Z. Yuanfang, Q.i. Ge, Enhanced multimaterial 4D printing with active hinges, Smart Mater. Struct. 27 (6) (2018) 065027, https://doi.org/10.1088/1361-665X/aabe63.